


## RESEARCH ARTICLE

## Symmetry dependent optical properties of zeolites: A quantum mechanical study

Mufasila Mumthaz Muhammed<sup>1</sup> | Fadi Sibai<sup>1</sup> | Ali J. Chamkha<sup>2</sup> |  
Junais Habeeb Mokkath<sup>3</sup> <sup>1</sup>American International University, Al Jahra, Kuwait<sup>2</sup>Faculty of Engineering, Kuwait College of Science and Technology, Kuwait City, Kuwait<sup>3</sup>Quantum Nanophotonics Simulations Lab, Department of Physics, Kuwait College of Science And Technology, Kuwait City, Kuwait

## Correspondence

Junais Habeeb Mokkath, Quantum Nanophotonics Simulations Lab, Department of Physics, Kuwait College of Science And Technology, Doha Area, 7th Ring Road, P.O. Box 27235, Kuwait City, Kuwait.  
Email: [j.mokath@kcst.edu.kw](mailto:j.mokath@kcst.edu.kw)

## Funding information

Kuwait College of Science And Technology (KCST)

## Abstract

The outstanding structural and chemical characteristics of zeolites (porous crystal forms of aluminosilicate oxides) are well known, but little is known about their optical properties. In this work, we examine the impact of symmetry on the optical characteristics of zeolites utilizing quantum simulations via time-dependent density functional theory. We demonstrate that zeolites with high symmetry (cubic ACO zeolite) absorb light in the visible spectrum, whereas zeolites with low symmetry (trigonal AFY zeolite) absorb light in the UV–vis region of the electromagnetic spectrum. Additionally, we reveal the nature of optical excitations by our analysis of the electron–hole distribution using transition density matrices. The zeolites also displayed significant variations in their electronic circular dichroism spectra, suggesting symmetry-driven modulations. This theoretical work offers crucial information about the optical properties of zeolites.

## KEYWORDS

optical properties, TDDFT, zeolites

## 1 | INTRODUCTION

Nanoporous materials exhibit outstanding features like high surface area and high porosity [1–11]. They have received a lot of interest in the fields of material science and materials engineering and are utilized in a variety of processes, for instance in gas separation, catalysis, and drug delivery, to name a few. The presence of nanopores of different size and shape enable them to exhibit novel features that are not present in the bulk material. Among the nanoporous materials, zeolites [12–21] (porous crystal forms of aluminosilicate oxides) are the most well-known and widely used materials due to their widespread availability, affordable price, and superior thermal, mechanical, and chemical durability. There are more than 200 zeolites reported with different chemical compositions and distinct framework topologies. Although a plethora of zeolites have been synthesized and chemically and structurally characterized [22–29], first-principles theoretical simulations investigating their optical features are still very scarce.

For the design and production of zeolite-based optical material, a thorough understanding of their optical properties is essential. To the best of our knowledge, quantum simulations that elucidate the optical characteristics of zeolites are scarce. This gap will be closed by the current quantum calculations. It is noteworthy that computational photochemistry's predictive ability has continuously grown over the past few years and that it is currently regarded as a crucial tool in scientific research. In this work, we want to comprehend how the optical properties of zeolites change in relation to modifications in shape or symmetry utilizing quantum simulations using the time-dependent density functional theory (TDDFT). We remark that quantum simulations are worthwhile since unlike classical simulations they precisely incorporate quantum effects [30–40]. TDDFT has become a very popular technique for the calculation of excited-state properties nowadays benefiting from its efficient numerical implementations. It has been implemented in both frequency domain (linear response TDDFT [*lr*-TDDFT] [41–47] technique based on the

Casida's equation solved in the basis of Kohn–Sham [KS] particle-hole transitions) and time domain (real-time TDDFT [rt-TDDFT] [48–52] technique based on the explicit propagation of the time-dependent KS equations).

The goal of this paper is to investigate how the underlying symmetry has a significant impact on the photoabsorption characteristics of zeolites. As a main result, we demonstrate that high symmetry zeolite exhibits photoabsorption in the visible region, whereas, lower symmetry zeolite exhibits photoabsorption in the UV–vis region of the electromagnetic spectrum. Electron–hole distribution in these materials (calculated via transition density matrices [TDMs]) and electronic circular dichroism (ECD) spectra provided important information regarding their optical excitations. The paper is organized as follows. In the Section 2, we describe the structural models and the computational method used. Results are presented and discussed in the Section 3 where we derive how the optical properties are influenced by the change in symmetry. We summarize our results in the Section 4.

## 2 | COMPUTATIONAL METHODOLOGY

The computational methodology used in this work is based on the DFT and *lr*-TDDFT method implemented in the Gaussian 16 [53, 54] software package. DFT and TDDFT methods are currently the most widely used techniques in computational material research due to the optimal balance of accuracy and computational power. Regarding the materials under investigation, we have taken into consideration two 48-atom zeolite structures, namely ACO and AFY (16 silicon atoms and 32 oxygen atoms), see Figure 1. In contrast to AFY zeolite, which has a lower symmetry trigonal structure, ACO zeolite has a high symmetry cubic structure. Si–O interatomic distance in both structures is 1.60 Å, as determined by the analysis of the radial distribution functions (RDFs:  $g(r) = \frac{1}{4\pi r^2} \frac{1}{N_p} \sum_{i=1}^N \sum_{j \neq i}^N \langle \delta(r - |r_i - r_j|) \rangle$ ). Regarding the DFT calculations, structure relaxations were carried out using an all-electron Pople double zeta basis set 6-31G [55–57]. The symmetry of the starting structures has been imposed during the structure relaxations. Although in principle an exact theory, in practice the accuracy of both DFT and TDDFT depends significantly on the employed exchange–correlation (XC) functional. We employed the CAM-B3LYP [58] range separated XC-functional (with 16% short-range and 65% long-range Hartree–Fock [HF] contributions). It is noteworthy that both local-density approximation [59] and generalized gradient approximation [60] XC-functionals consistently underestimate the excitation energies and charge transfer excitations. The issue of underestimating excitation energy and charge transfer excitations [61–64] has been successfully addressed in this regard by the use of the CAM-B3LYP XC-functional. It is noteworthy that accurate descriptions of valence excitations require full range-separated functionals [65–67] with the correct 100% HF asymptotic exchange. Additionally, we examined the impact of the HF exchange on the photoabsorption spectra (see Figure S1). More specifically, we compare the photoabsorption spectra of the ACO zeolite structure using four different methods (a) wB97x (16% HF exchange at short range and 100% HF exchange at long range); (b) CAM-B3LYP (19% HF exchange at short range and 65% HF exchange at long range); (c) PBE0 (25% HF exchange); and (d) HF method. It is noteworthy that different XC-functionals render qualitatively similar results.

Here is our computational approach. After performing DFT calculations for the ground state, photoabsorption spectra are calculated using the *lr*-TDDFT technique based on Casida's formulation [68–70]. This is the most popular *lr*-TDDFT implementation which involves setting up and solving an eigenvalue problem over a basis of single-particle excitations. In essence, Casida's technique expands the molecular KS orbitals as linear combinations of atomic functions and recasts the TDDFT problem in terms of diagonalizing a matrix  $\Omega$ . In practice, the KS equations are solved first,  $H_{KS}\phi_i = \varepsilon_i\phi_i$ . Then, the  $\Omega$  matrix is diagonalized,  $\Omega F_I = \omega_I^2 F_I$ , where the matrix elements of the  $\Omega$  matrix can be calculated from the KS

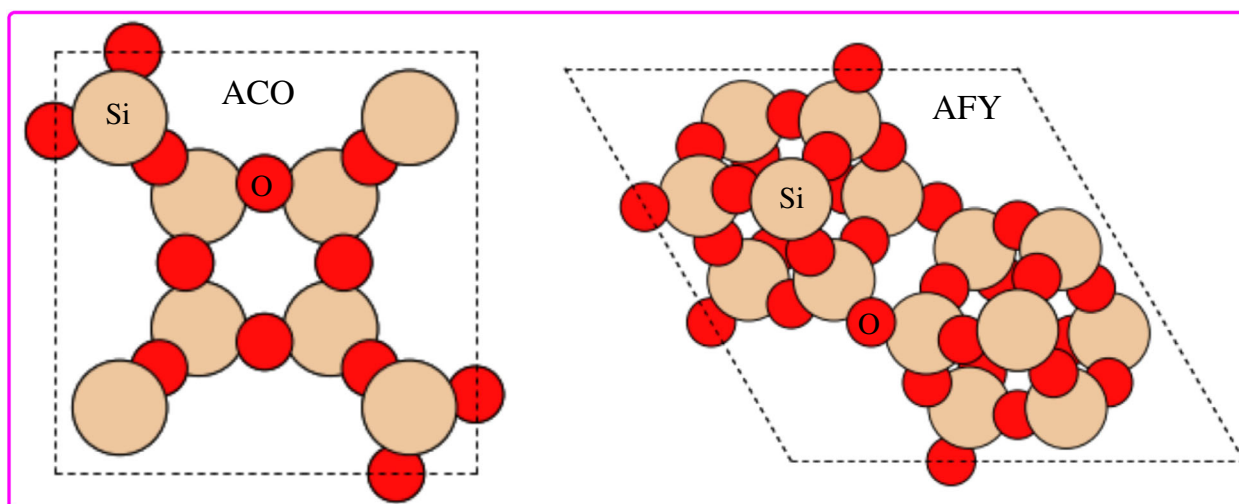


**FIGURE 1** ACO and AFY zeolite structures under investigation. Each structure consists of 48 atoms: 16 Si (gray) and 32 O (red)

orbitals and eigenvalues,  $\Omega_{ia,jb} = \delta_{ij}\delta_{ab}(\epsilon_a - \epsilon_i)^2 + 2\sqrt{\epsilon_a - \epsilon_i}K_{ia,jb}\sqrt{\epsilon_b - \epsilon_j}$  and the coupling matrix elements  $K_{ia,jb}$  are defined as  $K_{ia,jb} = \langle a|j|ib \rangle + \langle a|j|f_{\sigma}^{XC}|ib \rangle$ . The number of dipole-allowed KS transitions should be sufficient to cover the appropriate range in the photoabsorption spectrum. In order to plot the photoabsorption spectra of ACO and AFY zeolites in the energy range of 0–4.50 eV, we discovered that 200 transitions are required.

### 3 | RESULTS AND DISCUSSION

We begin our analysis-discussion starting with the photoabsorption spectra of ACO and AFY zeolite structures displayed in Figure 2. Zeolite systems are found to have distinctive optical characteristics. The photoabsorption spectrum of ACO zeolite appears in the visible portion of the electromagnetic spectrum in the energy range between 1 eV (1240 nm) and 3 eV (414 nm), with a dominating peak at about 2.42 eV contributing to the majority of the photoabsorption spectrum (with a high oscillator strength of 4.6). In a nutshell, the photoabsorption spectrum of ACO zeolite is characterized by four peaks, which are situated at  $\sim 1.77$ , 1.91, 2.39, and 2.42 eV and exhibit distinct fingerprints of its optically important electronic states. Note that in Figure 2, we have also provided (in the brackets) the main electronic transition contributing to the photoabsorption peaks. Although there are many transitions in Figure 2, transitions with high oscillator strengths (over 0.1) are specifically examined. The oscillator strengths of the 48th, 51st, 67th, and 71st transitions in ACO zeolite are larger than 0.1. The remaining transitions have oscillator strengths that are substantially lower than 0.1.

Comparing the photoabsorption characteristics of AFY zeolite to the (previously discussed) ACO case, significant differences can be seen. The different symmetry of the structures under investigation can be used to explain variations in the photoabsorption characteristics. Unlike the ACO photoabsorption spectrum, the AFY photoabsorption spectrum spans in the visible and ultraviolet region of the electromagnetic spectrum, from an energy range of 1 eV to the maximum considered energy range of 4.50 eV. In other words, the AFY photoabsorption spectrum spans the entire (considered) energy range. Figure 2 shows that AFY zeolite presents several transitions. Nevertheless, as mentioned before in the case of ACO zeolite, analyzing all these transitions cumbersome and thus, our analysis of AFY photoabsorption spectrum is restricted to a few selected

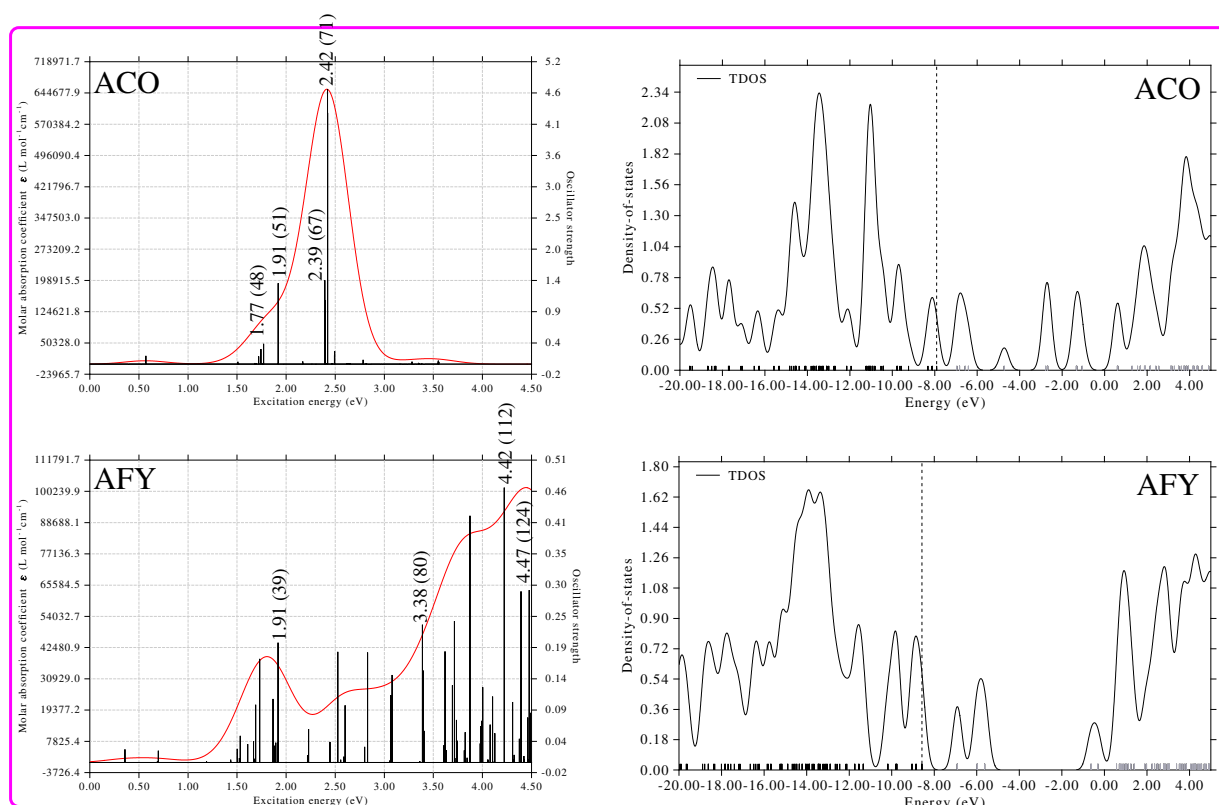


**FIGURE 2** Photoabsorption spectra of the zeolite structures ACO (top left) and AFY (bottom left) computed using time-dependent density functional theory (TDDFT). The photoabsorption spectra are broadened by a Gaussian smearing of width  $\sigma = 0.15$  eV. On the right side, the total density of states (TDOS) corresponding to each structure is displayed. In TDOS, the dashed line represents the highest occupied molecular orbital (HOMO)

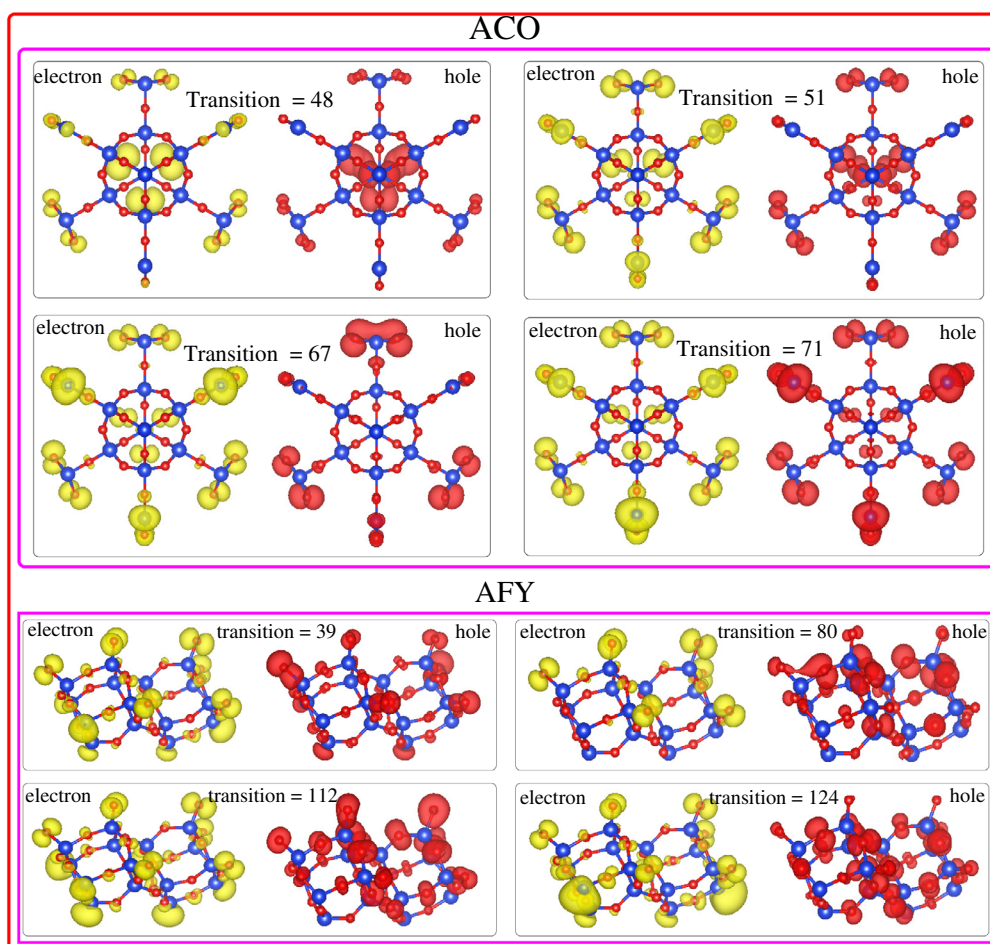


**FIGURE 3** Spatial distribution of electrons and holes corresponding to the different transitions (Figure 2) exhibited by ACO and AFY zeolite structures

transitions located at around 1.91, 3.38, 4.42, and 4.47 eV. Note that the oscillator strength of AFY transitions are significantly smaller in comparison to ACO oscillator strengths. This is associated with the change in reduced symmetry from ACO cubic to AFY trigonal. The total density of states (TDOS) corresponding to ACO and AFY zeolite structures are also shown in the right panel of Figure 2. The spread of the AFY photoabsorption spectrum to the ultraviolet region of the electromagnetic spectrum is presumably caused by a somewhat larger density of occupied and unoccupied electronic states near the Fermi level. It is important to compare the photoabsorption characteristics displayed in Figure 2 with the results that have been reported in the literature. Unfortunately, we have been unable to find even one theoretical or experimental paper that provided information on the photoabsorption spectra of pristine ACO and/or AFY zeolites. We anticipate that the findings of such experiment will be available soon. Furthermore, we anticipate that there will be some slight differences between the experimental data and the theoretical results (energetic position and intensity of the photoabsorption peaks). This is due to the fact that the present theoretical calculations are performed in vacuum with no variations in pH values or ionic strength of the solvent medium.

To further understand the nature of the photoabsorption peaks of ACO and AFY zeolite structures, we analyze and discuss next the electron and hole distributions corresponding to the selected transitions shown in Figure 2. The spatial distribution profile of electrons and holes offers a way to assign excitations, whether localized or charge transfer without the need for orbital inspection, offers subtle information about the type of excitation. Large disparities in their spatial distribution imply a significant charge transfer, whereas electron and hole densities that are very equal indicate only a minor charge transfer. The electron and hole distributions of the ACO zeolite for transitions 48, 51, 67, and 71, as well as the electron and hole distributions of the AFY zeolite structure for transitions 39, 80, 112, and 124, are shown in Figure 3. We start by analyzing how electrons and holes are distributed in ACO zeolite (see the top panel of Figure 3). One discovers that there is almost no significant gap between the centroids of electrons and holes in any transition and that they almost always coincide. In other words, there is a tremendous amount of overlap between electrons and holes. Our visual examination of the electron and hole distributions corresponding to the various transitions in ACO leads us to believe that each transition is a local excitation, and that this is what mostly contributes to the photoabsorption spectrum. The distributions of electrons and holes associated with the transitions in the AFY zeolite structure are next discussed (see the bottom panel of Figure 3).

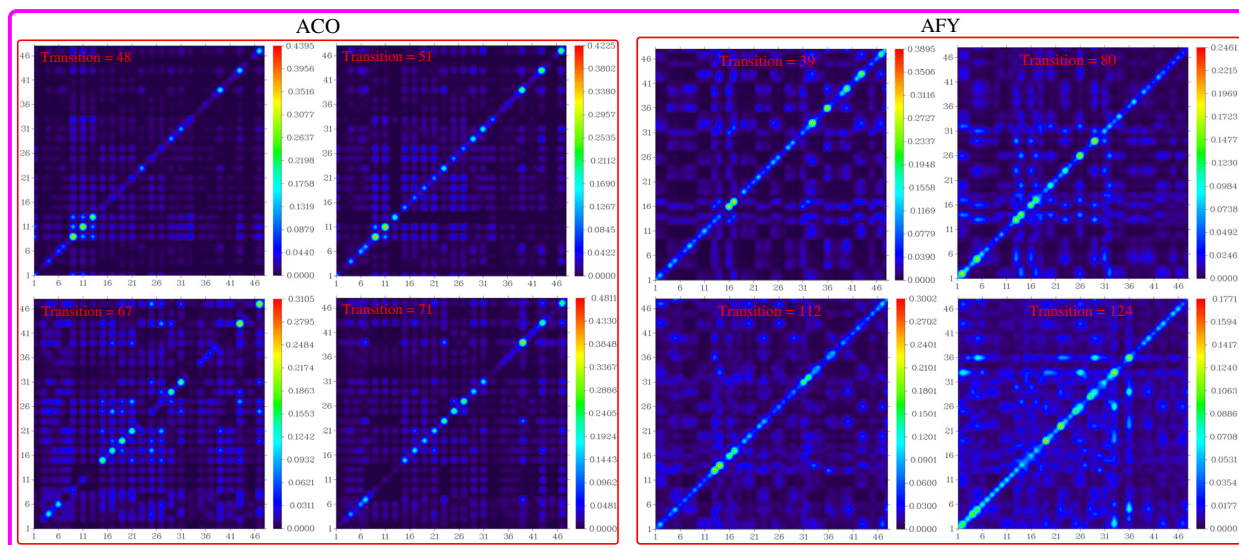


**FIGURE 4** Transition density matrices (TDMs) representing different optical transitions in ACO (left panel) and AFY (right panel) zeolite structures. The sizes of plotted matrices are 48 times 48 (equal to the total number of atoms). The color maps are given on the right side of each TDM plots

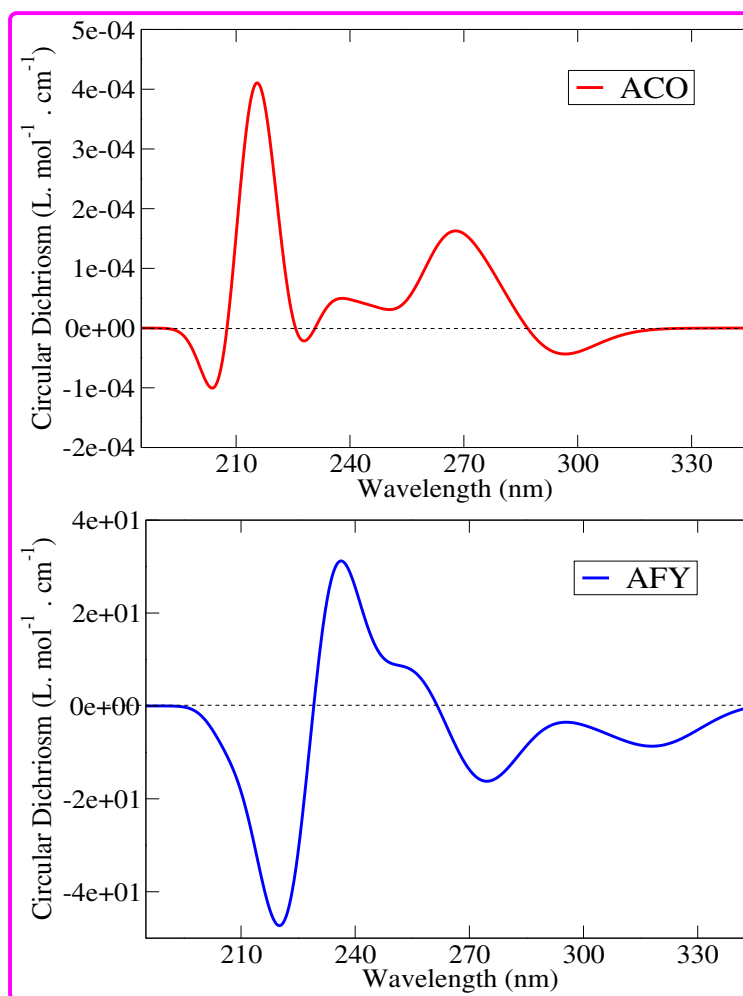


**FIGURE 5** Time-dependent density functional theory (TDDFT) calculated electronic circular dichroism spectra of ACO zeolite (top) and AFY zeolite (bottom)

Evidently, in contrast to the local excitations observed in the ACO zeolite structure, the excitations in the AFY structure are primarily local but also include significant charge transfer contributions. The centroids of electrons and holes, in particular, are shown to be significantly apart from one another.

Next, we analyze-discuss the TDMs [71–76] corresponding to the selected transitions highlighted in Figure 2. We point out that TDMs offer a unique two-dimensional color-filled map that shows the distribution of electron–hole pairs and enables one to determine the delocalization and coherence lengths of those pairs. TDMs, in particular, make it possible to determine which atoms are most impacted by transitions and which atom pairs exhibit significant coherence when an electron transits. Note that charge transfer between atoms is represented by off-diagonal contributions, whereas local excitations are mapped on the main diagonal running from the lower left to the upper right. The value appears brighter on the map if the effect is stronger during excitation. In Figure 4, we display TDMs for the transitions for ACO and AFY zeolite that were highlighted in Figure 2. TDMs corresponding to various excitations (48, 51, 67, and 71) in the case of ACO zeolite (see the left panel in Figure 4) show more or less having similar characteristics. More specifically, bright spots, albeit a few can be spotted on the off-diagonal, are almost symmetric with regard to the main diagonal. However, it is possible to draw the conclusion that ACO excitations are primarily local in nature. In the case of AFY zeolite, the situation is different. One discovers that transitions 80 and 124 are made up of both local and charge transfer excitations, in contrast to transitions 39 and 112, which are localized. The bright spots are found to be present at transitions 80 and 124 on both the main diagonal (running from the bottom left to the upper right) and off-diagonal (charge transfer from Si to O atoms). Overall, we note that TDMs offer a compelling substitute for the conventional quantum-chemical characterization of photoexcitation processes based on molecular orbitals.

In Figure 5 we present and contrast the ECD spectrum of ACO and AFY zeolites. ECD is a phenomena that results from chiral systems interacting with circularly polarized light. More particular, chiral systems absorb circularly polarized light differently for right- and left-handed systems. ECD spectroscopy is used to examine this distinction. The difference in molar extinction coefficient is a frequently used experimental metric to assess ECD spectra:  $\Delta\epsilon(\omega) = \frac{16\pi N_A}{3\ln(10)10^9} \frac{2\pi}{hc} \omega R(\omega)^{cgs}$ . Here,  $\omega$  is the energy of the incident light,  $c$  is the speed of light,  $\hbar$  is the reduced Planck constant,  $N_A$  is Avogadro's constant, and  $R(\omega)^{cgs}$  is the rotatory strength in cgs units. More recently, TDDFT techniques have been successfully employed in ECD calculations [77, 78]. In contrast to the ECD spectra of AFY zeolite, Figure 5 demonstrates how weak the ECD spectrum of ACO zeolite is. This can be due to the ACO structure's high cubical symmetry. Both positive and negative bands can be seen in the spectra of ACO zeolite, as seen in Figure 5. The strongest positive band (between 210 and 230 nm) consists of a single dominant peak. Additionally, there are a few positive bands that are visible at between 235 and 270 nm. Negative bands can also be found at wavelengths of about 200, 230, and 290 nm. In summary, the ECD spectra of the ACO structure are very weak, and it may be quite challenging to measure them experimentally. Positive and negative bands are very strong and powerful in the case of AFY zeolite. At around 235 nm, there is a strong positive band, and at about 220 nm, there is a strong negative band. At 275 and 320 nm, there are a few other negative bands that are not as strong. Overall, the AYF zeolite's ECD spectrum is robust and is easy to measure in an ECD experiment.

## 4 | CONCLUSIONS AND OUTLOOK

In conclusion, we have shown that symmetry and the optical characteristics of zeolites are related. We utilize TDDFT to perform first-principle quantum simulations. We show that the underlying symmetry significantly affects the zeolite photoabsorption properties. We find that zeolites with high symmetry (cubic ACO) absorb light in the visible range, whereas zeolites with low symmetry (trigonal AFY) absorb light in the UV and visible range. Our analysis of the optical excitations using TDMs helped us gain a better understanding of the electron–hole distribution in these materials. Additionally, the ECD spectrum of zeolites were also computed. We discovered striking differences in ECD spectra that suggest symmetry-driven modulations. In our view, the calculated results will contribute to a better understanding of zeolite optical excitations.

### AUTHOR CONTRIBUTIONS

**Mufasila Mumthaz Muhammed:** Conceptualization; data curation; formal analysis; funding acquisition; investigation; methodology; project administration; resources; writing – original draft; writing – review and editing. **Fadi Sibai:** Supervision; writing – original draft. **Ali J. Chamkha:** Supervision; validation. **Junais Habeeb Morkath:** Software; supervision; writing – original draft; writing – review and editing.

### ACKNOWLEDGMENT

The research reported in this publication was supported by funding from Kuwait College of Science And Technology (KCST).

### DATA AVAILABILITY STATEMENT

The data that support the findings of this study are available from the corresponding author upon reasonable request.

### ORCID

Junais Habeeb Morkath  <https://orcid.org/0000-0001-8889-5889>

## REFERENCES

- [1] R. W. Broach, *Zeolites in Industrial Separation and Catalysis*, John Wiley Sons, Ltd, Kuwait **2010**, p. 27.
- [2] S. S.-Y. Chui, S. M.-F. Lo, J. P. H. Charmant, A. G. Orpen, I. D. Williams, *Science* **1999**, 283, 1148.
- [3] H. M. El-Kaderi, J. R. Hunt, J. L. Mendoza-Cortés, A. P. Côté, R. E. Taylor, M. O'Keeffe, O. M. Yaghi, *Science* **2007**, 316, 268.
- [4] R. Banerjee, A. Phan, B. Wang, C. Knobler, H. Furukawa, M. O'Keeffe, O. M. Yaghi, *Science* **2008**, 319, 939.
- [5] W. Lu, D. Yuan, D. Zhao, C. I. Schilling, O. Plietzsch, T. Muller, S. Bräse, J. Guenther, J. Blümel, R. Krishna, Z. Li, H.-C. Zhou, *Chem. Mater.* **2010**, 22, 5964.
- [6] N. W. Ockwig, O. Delgado-Friedrichs, M. O'Keeffe, O. M. Yaghi, *Acc. Chem. Res.* **2005**, 38, 176 PMID: 15766236.
- [7] O. Delgado-Friedrichs, M. O'Keeffe, O. M. Yaghi, *Phys. Chem. Chem. Phys.* **2007**, 9, 1035.
- [8] A. Schoedel, M. Li, D. Li, M. O'Keeffe, O. M. Yaghi, *Chem. Rev.* **2016**, 116, 12466 PMID: 27627623.
- [9] G. C. Lisensky, O. M. Yaghi, *J. Chem. Educ.* **2022**, 99, 1998.
- [10] Z. Ji, R. Freund, C. S. Diercks, P. Hirschle, O. M. Yaghi, S. Wuttke, *Adv. Mater.* **2021**, 33, 2103808.
- [11] Z. Ji, H. Wang, S. Canossa, S. Wuttke, O. M. Yaghi, *Adv. Funct. Mater.* **2020**, 30, 2000238.
- [12] Y. Li, J. Yu, *Chem. Rev.* **2014**, 114, 7268.
- [13] Y. Li, J. Yu, *Nat. Rev. Mater.* **2021**, 6, 1156.
- [14] S. T. Wilson, B. M. Lok, C. A. Messina, T. R. Cannan, E. M. Flanigen, *J. Am. Chem. Soc.* **1982**, 104, 1146.
- [15] N. Rangnekar, N. Mittal, B. Elyassi, J. Caro, M. Tsapatsis, *Chem. Soc. Rev.* **2015**, 44, 7128.
- [16] C. Martínez, A. Corma, *Coord. Chem. Rev.* **2011**, 255, 1558.
- [17] Y. Chai, W. Shang, W. Li, G. Wu, W. Dai, N. Guan, L. Li, *Adv. Sci.* **2019**, 6, 1900299.
- [18] Q. Zhang, J. Yu, A. Corma, *Adv. Mater.* **2020**, 32, 2002927.
- [19] M. Y. Jeon, D. Kim, P. Kumar, P. S. Lee, N. Rangnekar, P. Bai, M. Shete, B. Elyassi, H. S. Lee, K. Narasimharao, S. N. Basahel, S. al-Thabaiti, W. Xu, H. J. Cho, E. O. Fetisov, R. Thyagarajan, R. F. DeJaco, W. Fan, K. A. Mkhoyan, J. I. Siepmann, M. Tsapatsis, *Nature* **2017**, 543, 690.
- [20] E. M. Gallego, M. T. Portilla, C. Paris, A. León-Escamilla, M. Boronat, M. Moliner, A. Corma, *Science* **2017**, 355, 1051.
- [21] P. Zhao, L. Ye, Z. Sun, B. T. W. Lo, H. Woodcock, C. Huang, C. Tang, A. I. Kirkland, D. Mei, S. C. Edman Tsang, *J. Am. Chem. Soc.* **2018**, 140, 6661.
- [22] M. Dusselier, M. E. Davis, *Chem. Rev.* **2018**, 118, 5265.
- [23] Q. Zhang, S. Gao, J. Yu, *Chem. Rev.* **2022**, 36049046.
- [24] K. Lu, Y. Fan, J. Huang, J. Wang, H. Xu, J. Jiang, Y. Ma, P. Wu, *J. Am. Chem. Soc.* **2021**, 143, 20569.
- [25] J. B. Nicholas, *Top. Catal.* **1997**, 4, 157.
- [26] B. Mounsef Jr., S. F. de Alcântara Morais, A. P. de Lima Batista, L. W. de Lima, A. A. C. Braga, *Phys. Chem. Chem. Phys.* **2021**, 23, 9980.
- [27] X. Rozanska, T. Demuth, F. Hutschka, J. Hafner, R. van Santen, *J. Phys. Chem. B* **2002**, 106, 3248.
- [28] G. Jajko, P. Kozyra, M. Strzempek, P. Indyka, M. Zajac, S. Witkowski, W. Piskorz, *Molecules* **2021**, 26, 3566.
- [29] Y. Mao, Z. Wang, H.-F. Wang, P. Hu, *ACS Catal.* **2016**, 6, 7882.
- [30] W. P. Halperin, *Rev. Mod. Phys.* **1986**, 58, 533.
- [31] E. Townsend, G. W. Bryant, *Nano Lett.* **2012**, 12, 429 PMID: 22181554.
- [32] P. Zhang, J. Feist, A. Rubio, P. García-González, F. J. García-Vidal, *Phys. Rev. B* **2014**, 90, 161407.
- [33] J. Zuloaga, E. Prodan, P. Nordlander, *Nano Lett.* **2009**, 9, 887 PMID: 19159319.
- [34] J. H. Morkkath, J. Henzie, *J. Mater. Chem. C* **2017**, 5, 4379.
- [35] J. H. Morkkath, *Phys. Chem. Chem. Phys.* **2018**, 20, 51.
- [36] J. H. Morkkath, *Phys. Chem. Chem. Phys.* **2022**, 24, 12389.
- [37] J. H. Morkkath, *Phys. E* **2021**, 129, 114670.
- [38] J. H. Morkkath, *Chem. Phys. Lett.* **2020**, 758, 137905.
- [39] J. H. Morkkath, J. Henzie, *Phys. Chem. Chem. Phys.* **2020**, 22, 1416.
- [40] J. H. Morkkath, *Phys. Chem. Chem. Phys.* **2019**, 21, 26540.
- [41] C.-P. Hsu, S. Hirata, M. Head-Gordon, *J. Phys. Chem. A* **2001**, 105, 451.
- [42] D. W. Silverstein, N. Govind, H. J. J. van Dam, L. Jensen, *J. Chem. Theory Comput.* **2013**, 9, 5490.
- [43] J. Neugebauer, *J. Chem. Phys.* **2007**, 126, 134116.
- [44] S. Grimme, *J. Chem. Phys.* **2013**, 138, 244104.
- [45] T. A. Niehaus, S. Suhai, F. Della Sala, P. Lugli, M. Elstner, G. Seifert, T. Frauenheim, *Phys. Rev. B* **2001**, 63, 085108.
- [46] J. H. Morkkath, *New J. Chem.* **2019**, 43, 18268.
- [47] M. M. Muhammed, J. H. Morkkath, *New J. Chem.* **2019**, 43, 10774.
- [48] K. Yabana, G. F. Bertsch, *Phys. Rev. B* **1996**, 54, 4484.
- [49] K. Yabana, T. Nakatsukasa, J.-I. Iwata, G. F. Bertsch, *Phys. Status Solidi B* **2006**, 243, 1121.
- [50] T. Sander, G. Kresse, *J. Chem. Phys.* **2017**, 146, 064110.
- [51] J. Jornet-Somoza, J. Alberdi-Rodríguez, B. F. Milne, X. Andrade, M. A. L. Marques, F. Nogueira, M. J. T. Oliveira, J. J. P. Stewart, A. Rubio, *Phys. Chem. Chem. Phys.* **2015**, 17, 26599.
- [52] J. H. Morkkath, U. Schwingenschlögl, *J. Phys. Chem. C* **2013**, 117, 23938.
- [53] M. J. Frisch, G. W. Trucks, H. B. Schlegel, G. E. Scuseria, M. A. Robb, J. R. Cheeseman, G. Scalmani, V. Barone, G. A. Petersson, H. Nakatsuji, X. Li, M. Caricato, A. V. Marenich, J. Bloino, B. G. Janesko, R. Gomperts, B. Mennucci, H. P. Hratchian, J. V. Ortiz, A. F. Izmaylov, J. L. Sonnenberg, D. Williams-Young, F. Ding, F. Lipparini, F. Egidi, J. Goings, B. Peng, A. Petrone, T. Henderson, D. Ranasinghe, V. G. Zakrzewski, J. Gao, N. Rega, G. Zheng, W. Liang, M. Hada, M. Ehara, K. Toyota, R. Fukuda, J. Hasegawa, M. Ishida, T. Nakajima, Y. Honda, O. Kitao, H. Nakai, T. Vreven, K. Throssell, J. A. Montgomery Jr., J. E. Peralta, F. Ogliaro, M. J. Bearpark, J. J. Heyd, E. N. Brothers, K. N. Kudin, V. N. Staroverov, T. A. Keith, R. Kobayashi, J. Normand, K. Raghavachari, A. P. Rendell, J. C. Burant, S. S. Iyengar, J. Tomasi, M. Cossi, J. M. Millam, M. Klene, C. Adamo, R. Cammi, J. W. Ochterski, R. L. Martin, K. Morokuma, O. Farkas, J. B. Foresman, D. J. Fox, *Gaussian 16 Revision C.01*, Gaussian, Inc., Wallingford, CT **2016**.
- [54] R. Dennington, T. A. Keith, J. M. Millam, *GaussView Version 6*, Semichem, Inc., Shawnee Mission, KS **2019**.
- [55] W. J. Hehre, R. Ditchfield, J. A. Pople, *J. Chem. Phys.* **1972**, 56, 2257.

- [56] R. C. Binning Jr., L. A. Curtiss, *J. Comput. Chem.* **1990**, *11*, 1206.
- [57] V. A. Rassolov, J. A. Pople, M. A. Ratner, T. L. Windus, *J. Chem. Phys.* **1998**, *109*, 1223.
- [58] T. Yanai, D. P. Tew, N. C. Handy, *Chem. Phys. Lett.* **2004**, *393*, 51.
- [59] P. Hohenberg, W. Kohn, *Phys. Rev.* **1964**, *136*, B864.
- [60] J. P. Perdew, K. Burke, M. Ernzerhof, *Phys. Rev. Lett.* **1997**, *78*, 1396.
- [61] R. Kobayashi, R. D. Amos, *Chem. Phys. Lett.* **2006**, *420*, 106.
- [62] Z.-L. Cai, M. J. Crossley, J. R. Reimers, R. Kobayashi, R. D. Amos, *J. Phys. Chem. B* **2006**, *110*, 15624 PMID: 16884287.
- [63] M. S. Kodikara, R. Stranger, M. G. Humphrey, *ChemPhysChem* **2018**, *19*, 1537.
- [64] K. Okuno, Y. Shigeta, R. Kishi, H. Miyasaka, M. Nakano, *J. Photochem. Photobiol., A* **2012**, *235*, 29.
- [65] L. N. Anderson, M. B. Oviedo, B. M. Wong, *J. Chem. Theory Comput.* **2017**, *13*, 1656 PMID: 28339200.
- [66] A. E. Raeber, B. M. Wong, *J. Chem. Theory Comput.* **2015**, *11*, 2199 PMID: 26574420.
- [67] B. M. Wong, T. H. Hsieh, *J. Chem. Theory Comput.* **2010**, *6*, 3704 PMID: 21170284.
- [68] M. E. Casida, C. Jamorski, K. C. Casida, D. R. Salahub, *J. Chem. Phys.* **1998**, *108*, 4439.
- [69] E. R. Davidson, *J. Comput. Phys.* **1975**, *17*, 87.
- [70] R. E. Stratmann, G. E. Scuseria, M. J. Frisch, *J. Chem. Phys.* **1998**, *109*, 8218.
- [71] R. McWeeny, *Rev. Mod. Phys.* **1960**, *32*, 335.
- [72] S. Tretiak, V. Chernyak, S. Mukamel, *Chem. Phys. Lett.* **1996**, *259*, 55.
- [73] S. Tretiak, K. Igemenshchev, V. Chernyak, *Phys. Rev. B* **2005**, *71*, 033201.
- [74] Y. Li, C. Ullrich, *Chem. Phys.* **2011**, *391*, 157.
- [75] A. V. Luzanov, A. A. Sukhorukov, V. É. Umanskii, *Theor. Exp. Chem.* **1976**, *10*, 354.
- [76] S. Mai, F. Plasser, J. Dorn, M. Fumanal, C. Daniel, L. González, *Coord. Chem. Rev.* **2018**, *361*, 74.
- [77] E. Makkonen, T. P. Rossi, A. H. Larsen, O. Lopez-Acevedo, P. Rinke, M. Kuisma, X. Chen, *J. Chem. Phys.* **2021**, *154*, 114102.
- [78] C. Bannwarth, S. Grimme, *Comput. Theor. Chem.* **2014**, *1040-1041*, 45.

## SUPPORTING INFORMATION

Additional supporting information can be found online in the Supporting Information section at the end of this article.

**How to cite this article:** M. M. Muhammed, F. Sibai, A. J. Chamkha, J. H. Makkath, *Int. J. Quantum Chem.* **2023**, e27084. <https://doi.org/10.1002/qua.27084>